A slow earthquake sequence on the San Andreas fault

Alan T. Linde*, Michael T. Gladwin†, Malcolm J. S. Johnston‡, Ross L. Gwyther† & Roger G. Bilham§

* Department of Terrestrial Magnetism, Carnegie Institution of Washington, 5241 Broad Branch Road NW, Washington DC 20015, USA
† Commonwealth Scientific and Industrial Research Organisation, Queensland Center for Advanced Technologies, 2643 Moggill Road, Pinjarra Hills, Queensland 4069, Australia
‡ US Geological Survey, 345 Middlefield Road, Menlo Park, California 94025, USA
§ Department of Geological Sciences, University of Colorado, Boulder, Colorado 80309-0216, USA

EARTHQUAKES typically release stored strain energy on timescales of the order of seconds, limited by the velocity of sound in rock. Over the past 20 years, observations[1–13] and laboratory experiments[14] have indicated that rupture can also occur more slowly, with durations up to hours. Such events may be important in earthquake nucleation[15] and in accounting for the excess of plate convergence over seismic slip in subduction zones. The detection of events with larger timescales requires near-field deformation measurements. In December 1992, two borehole strainmeters close to the San Andreas fault in California recorded a slow strain event of about a week in duration, and we show here that the strain changes were produced by a slow earthquake sequence (equivalent magnitude 4.8) with complexity similar to that of regular earthquakes. The largest earthquakes associated with these slow events were small (local magnitude 3.7) and contributed negligible strain release. The importance of slow earthquakes in the seismogenic process remains an open question, but these observations extend the observed timescale for slow events by two orders of magnitude.

Our study area (Fig. 1) is located at the transition between locked and stably sliding segments of the San Andreas fault in central California. The fault to the north ruptured in the great 1906 earthquake, and to the south, fault slip occurs through creep and small (local magnitude $m_L \lesssim 3$) earthquakes. Our borehole instruments are a Sacks–Evertson strainmeter[16] (dilatometer) at site SRL (depth 138 m) and a Gladwin tensor (three-component) strainmeter[17] at SJT (146 m). The first instrument measures volume change (dilatation). The second measures horizontal deformation in three directions at 120°. These measurements are combined to give areal strain and two orthogonal shear strains. The data are collected by the US Geological Survey (USGS) in Menlo Park via satellite digital telemetry[18]. SRL is sampled every 10 minutes and SJT every 18 minutes. Another dilatometer at EVS, more distant from the fault, is in highly fractured rock which

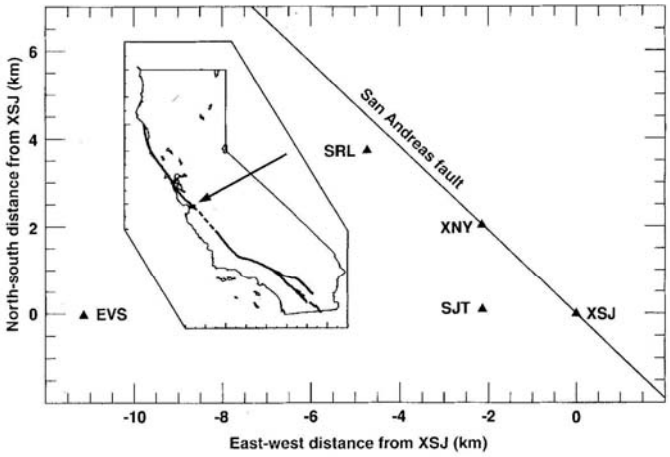

FIG. 1 Map of the location of borehole instruments SRL, SJT and EVS; of creepmeters XSJ and XNY, and of the San Andreas fault. The insert of California (large tick marks are for 1 degree of latitude and longitude) shows the site area (indicated by the arrow) and the main trace (heavy line) of the San Andreas fault. The dashed section south of the study area indicates the creeping part of the fault. Creepmeters span the fault and measure the relative displacement across it. Borehole strainmeters are located off the fault both to avoid installation in fault zone material and to allow sensitivity to deformation at depth on the fault.

gives low-quality data; these are not inconsistent with our models but are not valuable for constraining parameters. Surface slip on the fault near these instruments is monitored by two 10-m-long creepmeters that cross the fault obliquely[19,20].

In December 1992, the strainmeters recorded a strain excursion unique to the data since observations began in 1984. Figure 2 shows eight months of data from SRL and SJT starting about six months before the slow event. The large, slow strain change in December dominates the record. Also shown in Fig. 2 are the earthquakes located in the area approximately between SRL and SJT with magnitudes greater than or equal to 2.5.

Figure 3 shows 10 days of data (solid lines) from both instruments. These data have been linearly detrended, and tidal components and strain changes induced by atmospheric pressure have been removed[21]. Theoretical estimates of the ocean-loaded tidal amplitudes[22] have been used for calibration. Both instruments have a constant response to strain over all periods of interest. The slow changes began with a relatively rapid change on 11 December followed by slow, exponential-like changes over about 8 days, interrupted by relatively rapid changes on 12 December and on 14 December. These changes over time are indicative of a series of slow events, which we have labelled A to E.

Creep data (Fig. 3) from sites XNY[18] and XSJ[19] provide qualitative constraints for modelling. Creep events are different from slow earthquakes; they are due to the nonlinear failure of the near-surface materials (of depths less than a few hundred metres), perhaps in response to deeper slip[23–25]. At XSJ, there is no relative displacement across the fault until event E. At XNY, creep response to the deep slip was probably masked by left-lateral surface displacement, caused by heavy rain, which reversed to the tectonic right-lateral sense soon after event C. The slow strain event is not caused by precipitation; it is the only event of this type in 12 years of data (up to mid-1996), whereas there are comparable or larger amounts of rain every wet season in December–January.

One earthquake (m_L 3.1; number 1 in Figs 3, 4) occurred about two hours before the slow sequence began. Two earthquakes (m_L 3.3, 3.2; numbers 2, 3) occurred within the first and third sample intervals (on both instruments) showing slow strain changes. The next day two m_L 3.7 earthquakes (numbers 5, 6) took place during the first sample interval of large slow strain change on both instruments. Smaller earthquakes (including numbers 4 and 7) preceded and followed these more rapid changes. Coseismic strain changes for these earthquakes are negligible (a few nano-

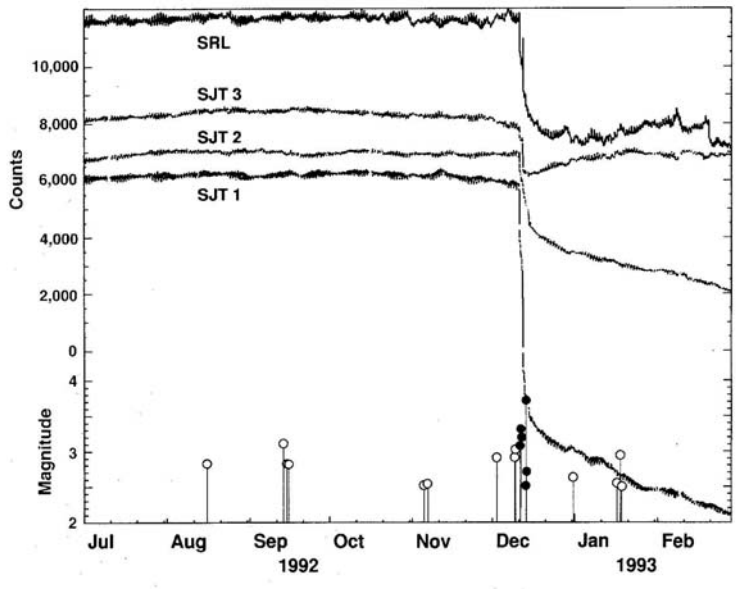

FIG. 2 Eight months of detrended data from SRL and from the three sensors of SJT. The sign of the data from SJT1 has been reversed. Short-term variations are the solid earth tides and some of the longer-term changes are due to variations in atmospheric pressure. The slow earthquake sequence in early December dominates the record. The range of the number of counts shows that the event is very well resolved. The lower part of the figure shows local earthquakes with magnitudes of at least 2.5; solid circles denote those that occurred during the time interval shown in Fig. 3. For about 10 days (see Fig. 3) the two strainmeters show excellent coherence. Slow deformation continued for about six months but the strain changes are less well correlated, suggesting that slow motion continued quasi-independently on smaller areas of the fault, or propagated past the along-fault limits given here (Fig. 4).

strain) compared with the observed strain changes (100–500 nanostrain) during those intervals. We include calculated[26] coseismic changes, but omitting them does not bias the model parameters for the slow events. Because of our sampling intervals (10 minutes for SRL, 18 minutes for SJT), we are unable to determine whether the earthquakes came before or after the initiation of the slow events. However, the absence of comparable seismicity, before and after this episode, is indicative of a causal connection between the occurrence of the slow events and earthquakes.

We restrict source models to pure right-lateral slip on areas of the San Andreas fault, taken as a vertical plane with strike N133.7 E. We search for the simplest solutions that provide satisfactory agreement with the strain data and consistency with the creep observations. As the strain changes are slow, we use the expressions given by Okada[26] for the deformations produced by a dislocation in an elastic half-space. We incorporate these into an algorithm for computing quasistatic, strain-change time series (at instrument depths) attributable to a slowly propagating rupture and/or a slow slip rise time. From the relative amplitudes of the strain changes, it is clear that we must have slip sources that are concentrated on the fault between SJT and SRL.

Consider first the strain events E and C. Event E is similar to a number of previous slow events which were modelled by Gladwin *et al.*[13] and we find a source (patch W in Fig. 4) with geometry similar to their model, although we have restricted the depth extent to 0.3 km. Slip of 5 mm, with slow rupture (average rupture velocity 0.2 ms^{-1}) to the southeast on W, provides good agreement with the strain changes at SJT (and with no change at SRL) and with the subsequent creep at XSJ. Our model calculations are shown in Fig. 3 as dashed curves.

Event C has a strain signal character at SRL which is different from that for the strains at SJT; reversal of strain direction requires rupture propagation which is slow compared with our sample interval of 10 minutes, such that a nodal line in the strain field passes through the station location as the source geometry changes. We have examined all possible model areas from just north of SRL to just south of SJT. The only viable solution found is slip of 2.8 cm on the patch marked Z; the rupture propagates slowly upwards (with exponentially decreasing rupture velocity, with average 0.35 ms^{-1}), resulting in a sign reversal of strain change at SRL and unidirectional changes at SJT.

For the remaining events, A, B and D, we minimize the number of free parameters by requiring a fixed source geometry with different slips for the different events. Amplitude ratios among the various strains cannot be satisfied by the simplest model of uniform slip over a single source area; we achieve good agreement by using adjoining areas X and Y (Fig. 4). We limit the top of Y to be 0.3 km from the surface, for consistency with lack of creep at XSJ until E; the top of X is 0.1 km deep. We have reasonable control of the extent along strike; the positions of the remote ends could be varied by about 1 km without significantly degrading the fit to the data. The boundary between X and Y could also be varied somewhat, but it probably could not be closer to XNY for the model to be consistent with the creep data. The top boundaries are well constrained; increasing their depth decreases the quality of the fit, and shallower depths conflict with the creep data. Our bottom depth control is much poorer. Both SJT and SRL are close to the fault and have little sensitivity to slip below about 4 km depth. We choose the minimum-area solution shown in Fig. 4 but equally good fits to the data could be obtained for sources with bottom extent anywhere in the depth range 4–8 km, or even deeper. Also sources of depths less than 4 km require less slip than those extending to 8 km because deeper parts of the source produce strains (at our sites) opposite in sign to those from the shallower parts. The quality of the fit decreases for depths less than 4 km. Our model (dashed curves in Fig. 3) has slip on X and Y of 3.7 and 2.9 mm, 5.6 and 3.4 mm, and 9.2 and 8.5 mm for events A, B and D respectively. The area of greatest slip is just above the cluster of larger earthquakes. Slow rupture propagation results in differences in shape between the recorded strains (for example as for event C). Because all strain signals have similar waveforms for A, for B and D, the simplest model has a rupture propagation time which is short compared with our sample interval of 10 min; the time variation results from slip rise time. The exponential time constants are 40 min for A, 15 h for B and 43 h for D.

The sequence of events in the model is that there was an initial episode (A) of slow slip over all of X and Y, followed by slower slip (B) over the same area. Then slow rupture propagated upwards over Z (event C); there may have been continuing slip over all of X and Y during this interval although our model does not include it. Slip then continued (more slowly) over X and Y (event D) and during that time, failure on patch W produced event E. This sequence is the simplest model we can find to provide reasonable agreement with the data.

The data provide unambiguous evidence for a slow earthquake

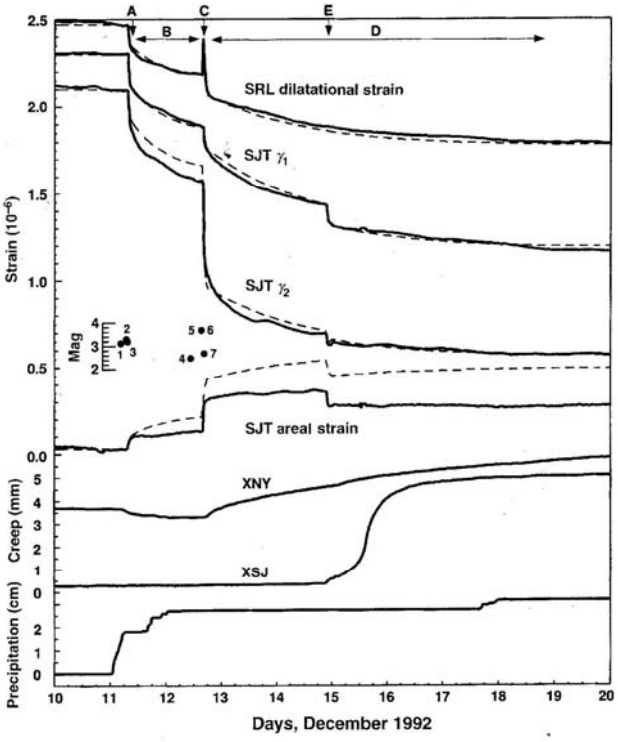

FIG. 3 Strain data (solid lines) from SRL and SJT for 10 days in December 1992 covering the duration of coherent slow changes. SRL records dilatational strain. From SJT we get γ_1 shear at N45 W (approximately fault-parallel) fault-normal shear γ_2, and areal strain. Earth tides and strain changes induced by atmospheric pressure have been removed; some residual tidal variations remain, including small changes before the initiation of the slow sequence. Creep data (XNY and XSJ) and precipitation are also shown. Earthquake times and magnitudes are shown in the insert numbered in order of origin time; there are two m_L 3.7 events on 12 December. The labels A–E indicate slow events within the sequence. Dashed curves are results from model calculations. Calculated coseismic changes are included but are not significant. The results are not significantly affected by reasonable errors in the site locations or by the non-verticality of the fault. The fit to SRL dilatation and to γ_1 shear is essentially perfect. We could improve the fit to areal strain by changing the amount of slip on X and Y (see text and Fig. 4) for events A, B and D without decreasing the fit to dilatation and γ_1, but the quality of the fit for γ_2 would decrease. This apparent discrepancy may be a result of using a homogenous Earth model in processing the data from the three sensors of SJT to produce the areal and shear strains. Preliminary finite-element modelling of the differences in material elastic constants on opposite sides of the fault indicates that area strain has been underestimated and that γ_2 has been overestimated.

sequence with significant complexity, not unlike that seen in regular earthquakes; such complex behaviour has not previously been observed for slow earthquakes. This event, with slip occurring over a period of about one week, extends the observed timescale for slow earthquakes by two orders of magnitude. We require slow slip over a large surface, with total moment equivalent to about a magnitude 4.8 earthquake. The occurrence of a slow earthquake on this part of the San Andreas fault may have some bearing on the nature of the transition from locked to creeping characteristic behaviour, but we cannot say exactly what this might be. The moment release of this event is small in comparison with the slip deficit proposed[27,28] for the San Andreas fault to the north of our study area. Earthquakes as large as magnitude 4.6 have occurred in this area; the capability of the fault to generate both slow and regular earthquakes is similar to that reported by Sacks *et al.*[6] for a fault in the Izu peninsula, Japan. Whereas the slowness of the Izu event could be ascribed primarily to slow rupture propagation, here most of the strain changes are attributed to slow slip rise time. Thus, not only can faults sustain ruptures over a wide range of timescales also the slowness can be in either or both of the rupture velocity and the time for slip to reach its final value. This slow sequence (with slip of a few centimetres) was accompanied by only small earthquakes, whereas the Izu slow event (slip of ~1 m) was followed by earthquakes as large as magnitude (m_b) 5.8. The slow precursor to the great (moment magnitude 9.5) 1960 Chile earthquake[1–4] was very large in extent, with slip of at least several metres.

These few observations seem to suggest a relation between the amount of slow redistribution of stress and the size of associated earthquakes, but additional observations of associated slow and regular earthquakes will be necessary before firm conclusions can be drawn. Unfortunately, slow events are difficult to detect; the total surface displacement generated by this slow sequence would have been barely detectable by Global Positioning System (GPS) receivers at our sites. As there are relatively few arrays of borehole strainmeters, and signal amplitudes decrease rapidly with increasing distance from the source, progress in determining the role of slow earthquakes in the seismogenic process is likely to be slow. □

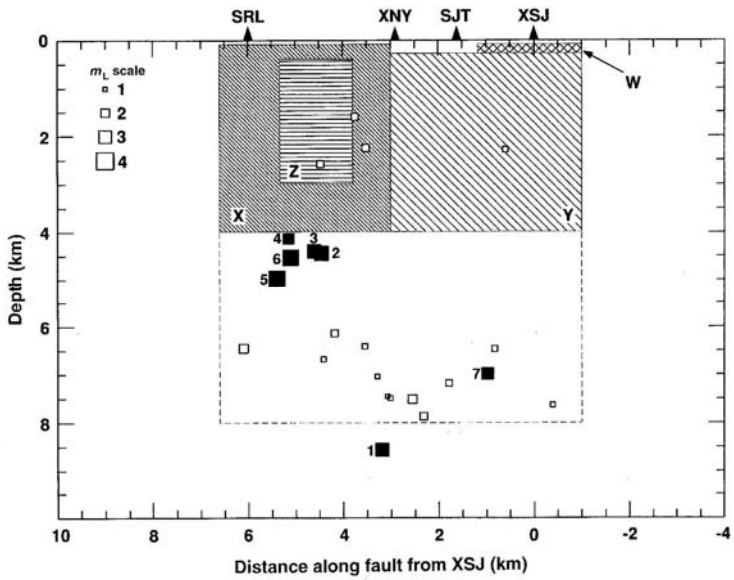

FIG. 4 Vertical section in the local strike direction of the San Andreas fault. Earthquakes are shown as filled squares for events with magnitudes ⩾2.5 (numbered as in Fig. 3), and open squares for smaller events; areas of these events are much smaller than for the slow slip. XSJ and XNY show the locations of creepmeters; SRL and SJT sites are shown projected onto the fault. Shaded areas are those used for the model calculations. Aseismic slip in X and Y corresponds to strain events A, B and D. Aseismic slip on Z and W corresponds to events C and D respectively. Dashed lines indicate that the source depths for X and Y could extend to 8 km.

Received 28 March; accepted 17 July 1996.

1. Kanamori, H. & Cipar, J. *Phys. Earth Planet. Int.* **9,** 127–136 (1974).
2. Kanamori, H. & Anderson, D. L. *J. Geophys. Res.* **80,** 1075–1078 (1975).
3. Cifuentes, I. L. & Silver, P. G. *J. Geophys. Res.* **94,** 643–663 (1989).
4. Linde, A. T. & Silver, P. G. *Geophys. Res. Lett.* **16,** 1305–1308 (1989).
5. Sacks, I. S., Suyehiro, S., Linde, A. T. & Snoke, J. A. *Nature* **275,** 599–602 (1978).
6. Sacks, I. S., Linde, A. T., Snoke, J. A. & Suyehiro, S. *Earthquake Prediction: An International Review* Maurice Ewing Ser. Vol. 4 (eds Simpson, B. W. & Richards, P. G.) 617–628 (AGU, Washington DC, 1981).
7. Sacks, I. S., Linde, A. T., Snoke, J. A. & Suyehiro, S. *Tectonophys.* **81,** 311–318 (1982).
8. Beroza, G. C. & Jordan, T. H. *J. Geophys. Res.* **95,** 2485–2510 (1990).
9. Ihmle, P. F. & Jordan, T. H. *Science* **266,** 1547–1551 (1994).
10. Satake, K. & Kanamori, H. *J. Geophys. Res.* **82,** 5692–5697 (1977).
11. Kanamori, H. & Kikuchi, M. *Nature* **361,** 714–716 (1993).
12. Kawasaki, I. *et al. J. Phys. Earth* **43,** 105–116 (1995).
13. Gladwin, M. T., Gwyther, R. L., Hart, R. H. G. & Breckenridge, K. *J. Geophys. Res.* **99,** 4559–4565 (1994).
14. Kato, K., Kusunose, K., Yamamoto, K. & Hirasawa, T. *J. Phys. Earth* **39,** 461–476 (1991).
15. Dieterich, J. H. & Kilgore, B. D. *Proc. Natl Acad. Sci. USA* **93,** 3787–3794 (1996).
16. Sacks, I. S., Suyehiro, S., Evertson, D. W. & Yamagishi, Y. *Pap. Meteorol. Geophys.* **22,** 195–207 (1971).
17. Gladwin, M. T. *Rev. Sci. Instrum.* **55,** 2011–2016 (1984).
18. Silverman, S., Mortensen, C. & Johnston, M. J. S. *Bull. Seismol. Soc. Am.* **79,** 189–198 (1989).
19. Behr, J., Bilham, R., Bodin, P., Burford, R. O. & Burgmann, R. *Geophys. Res. Lett.* **17,** 1445–1448 (1990).
20. Duffield, W. A. & Burford, R. O. *J. Res. U. S. Geol. Surv.* **1,** 569–577 (1973).
21. Ishiguro, M., Sato, T., Tamura, Y. & Ooe, M. *Proc. Inst. of Stat. Math.* **32,** 71–85 (1984).
22. Sato, T. & Hanada, H. *Publ. Int. Latitude Observ., Mizusawa* **18,** 29–47 (1984).
23. Johnston, M. J. S., McHugh, S. & Burford, R. O. *Nature* **260,** 691–693 (1976).
24. Goulty, N. R. & Gilman, R. *J. Geophys. Res.* **83,** 5415–5419 (1978).
25. Ruina, A. *J. Geophys. Res.* **88,** 10359–10370 (1983).
26. Okada, Y. *Bull. Seismol. Soc. Am.* **82,** 1018–1040 (1992).
27. Bodin, P. & Bilham, R. *U. S. Gol. Survey Prof. Pap.* **(1550-F)** 91–101 (1994).
28. Jaume, S. C. & Sykes, L. R. *J. Geophys. Res.* **101,** 765–789 (1996).

ACKNOWLEDGEMENTS. We thank D. Myren for helping to operate the SRL station, S. Silverman and K. Breckenridge for maintaining data acquisition files, and G. Beroza for reviewing the manuscript.

CORRESPONDENCE should be addressed to A.T.L. (e-mail:linde@dtm.ciw.edu).